Published in final edited form as:
J Neurosci. 2008 December 10; 28(50): 13629–13639. doi:10.1523/JNEUROSCI.4429-08.2008.

Stimulus-timing-dependent plasticity of cortical frequency representation

Johannes C Dahmen, **Douglas EH Hartley**, and **Andrew J King**
Department of Physiology, Anatomy and Genetics, Sherrington Building, University of Oxford, Parks Road, Oxford OX1 3PT, United Kingdom

Abstract

Adult cortical circuits possess considerable plasticity, which can be induced by modifying their inputs. One mechanism proposed to underlie changes in neuronal responses is spike-timing-dependent plasticity (STDP), an up- or down-regulation of synaptic efficacy contingent upon the order and timing of pre- and postsynaptic activity. The repetitive and asynchronous pairing of a sensory stimulus with either another sensory stimulus or current injection can alter the response properties of visual and somatosensory neurons in a manner consistent with STDP. To examine whether such plasticity also exists in the auditory system, we recorded from neurons in the primary auditory cortex of anesthetized and awake adult ferrets. The repetitive pairing of pure tones of different frequencies induced shifts in neuronal frequency selectivity, which exhibited a temporal specificity akin to STDP. Only pairs with stimulus onset asynchronies of 8 or 12 ms were effective and the direction of the shifts depended upon the order in which the tones within a pair were presented. Six hundred stimulus pairs (lasting ~70 s) were enough to produce a significant shift in frequency tuning and the changes persisted for several minutes. The magnitude of the observed shifts was largest when the frequency separation of the conditioning stimuli was < ~1 octave. Moreover, significant shifts were found only in the upper cortical layers. Our findings highlight the importance of millisecond-scale timing of sensory input in shaping neural function and strongly suggest STDP as a relevant mechanism for plasticity in the mature auditory system.

Keywords

auditory cortex; ferret; sound frequency tuning; spike-timing-dependent plasticity; conditioning

Introduction

The auditory system exhibits a remarkable degree of plasticity, both during development and in later life (Dahmen and King, 2007). Various experimental manipulations can alter the neural representation of a sound. These include changing the statistics of the acoustic environment (Zhang et al., 2001; Cheung et al., 2005; Norena et al., 2006; de Villers-Sidani et al., 2007), pairing acoustic with neuromodulatory signals (Bakin and Weinberger, 1996; Kilgard and Merzenich, 1998; Bao et al., 2001; Manunta and Edeline, 2004; Froemke et al., 2007), manipulating the behavioral significance of a sound (Recanzone et al., 1993; Ohl et al., 2001; Fritz et al., 2003; Blake et al., 2006; Polley et al., 2006; Schnupp et al., 2006), misaligning auditory and visual input (King et al., 1988; Knudsen and Brainard, 1991) and damaging the sensory periphery (Kamke et al., 2005).

Correspondence: Andrew J King PhD, Department of Physiology, Anatomy and Genetics, Sherrington Building, University of Oxford, Parks Road, Oxford OX1 3PT, UK Email: andrew.king@dpag.ox.ac.uk.

Europe PMC Funders Author Manuscripts

The mechanisms underlying activity-dependent changes in auditory response properties remain largely unexplored. Some kinds of plasticity may require structural changes involving the formation and elimination of synapses, whereas others may be mediated by alterations in synaptic strength. One way to regulate synaptic efficacy is by controlling the timing of pre- and postsynaptic activity. When presynaptic spikes precede postsynaptic spikes by up to tens of milliseconds synaptic transmission is strengthened, whereas the reverse activity pattern weakens the synapse. Since the initial discovery of this phenomenon (Markram et al., 1997; Zhang et al., 1998), spike-timing-dependent plasticity (STDP) has been demonstrated in numerous species, neural structures and cell types (Caporale and Dan, 2008).

STDP was first observed by directly controlling pre- and postsynaptic activity through precisely-timed current injections in slices and cell cultures. Attempts to control spiking by sensory stimulation *in vivo* have revealed that STDP can alter neuronal response properties, although its expression differs from that seen *in vitro*. While modifications of response properties in cat visual cortex (Schuett et al., 2001; Yao and Dan, 2001; Fu et al., 2002) through precisely-timed sensory stimuli were attributed to STDP because of their bidirectionality and temporal specificity, a direct link between *in vivo* STDP at the synaptic level and altered sensory representations was demonstrated only recently (Meliza and Dan, 2006; Mu and Poo, 2006; Vislay-Meltzer et al., 2006; Jacob et al., 2007). STDP has also been implicated in deprivation-induced map plasticity in visual (Young et al., 2007) and somatosensory cortex (Celikel et al., 2004), and in changes in the excitability of human motor (Wolters et al., 2003) and somatosensory (Wolters et al., 2005) cortex. Moreover, the same asynchronous pairing of visual stimuli that modifies orientation selectivity (Yao and Dan, 2001) or receptive field position (Fu et al., 2002) in cat visual cortex can induce corresponding perceptual changes in humans.

Given the importance of precise spike timing and extensive evidence for plasticity in the auditory system, it is surprising that there is presently no evidence that spike-timing-dependent synaptic modifications can affect the response properties of auditory neurons. Here we show that the relative timing of tones of different frequencies can control cortical frequency plasticity in a manner consistent with STDP.

Materials and Methods

Animal preparation

A total of 12 adult pigmented ferrets (*Mustela putorius furo*) were used in this study, 10 for recordings under anesthesia and 2 for recordings in the alert state. All surgical procedures were approved by the local ethical review committee and licensed by the UK Home Office.

In preparation for acute electrophysiological recordings, animals were sedated with an i.m. injection of medetomidine hydrochloride (Domitor; Pfizer Ltd.) and, after insertion of an i.v. cannula, maintained under anesthesia with continuous infusions of medetomidine hydrochloride (22 μg/kg/hr) and ketamine hydrochloride (5 mg/kg/hr, Ketaset; Fort Dodge Animal Health Ltd.) in a 0.9% saline solution supplemented with 5% glucose. A single, s.c. dose of 0.06 mg/kg/h atropine sulphate (C-Vet Veterinary Products) was provided, along with 0.5 mg/kg dexamethasone (Dexadreson; Intervet UK Ltd.) approximately every 12 hours, in order to reduce the risk of bronchial secretions and cerebral oedema, respectively. The animals were intubated and artificially ventilated with oxygen. End-tidal CO_2 and heart rate were monitored and body temperature was maintained at 38°C using a rectal probe coupled to a heating blanket. The skull was exposed and a stainless steel bar attached with stainless steel screws and dental cement above the mid-sagittal ridge. A craniotomy was made over the left or right middle ectosylvian gyrus (MEG) to expose the primary auditory

cortex (A1). The dura was removed and a 1.5% agar solution applied to protect the cortical surface and improve recording stability.

For awake electrophysiological recordings, animals were first conditioned over several days using water rewards to enter a plastic tube inside which they were to remain during the recording sessions. Once this phase was complete, the animals were anesthetized with medetomidine hydrochloride and ketamine hydrochloride and intubated. Under aseptic conditions, a portion of each temporal muscle was removed and a craniotomy made over the left and right MEG. Bilateral stainless steel recording chambers and a central head fixation socket were then attached with screws and Super-Bond C & B dental adhesive resin cement (Sun Medical Co. Ltd.). Analgesia (0.15 ml i.m. injection of of buprenorphine hydrochloride; Alstoe Animal Health) was provided both during and after the surgery. Recording sessions commenced several days later once the animals were fully recovered.

Electrophysiology and stimulus presentation

All electrophysiological recordings were carried out in a sound-attenuated chamber (Industrial Acoustics Company, Winchester, UK).

In the anesthetized ferrets, single-shank silicon probe electrodes (Neuronexus Technologies) with 16 recording sites spread over a length of 1.5 mm were used, so that units could be recorded simultaneously from different cortical layers. Stimuli were presented diotically through a pair of earphones (Panasonic, RP-HV298) attached to otoscope speculae that were inserted into each ear canal. These drivers were calibrated before each experiment to ensure that they produced a flat (±2 dB) frequency response between 500 Hz and 25 kHz.

For recordings carried out in the alert state, the animal was placed in a cylindrical plastic tube to restrict its body movements with its head attached to a metal bar. Stimuli were presented from a loudspeaker (Audax TWO25MO) placed in front of the animal and recordings were made with single tungsten-in-glass microelectrodes (Thomas Recording) inserted through the intact dura. Water was provided at regular intervals during these recording sessions.

Neural signals were band-pass filtered (500 Hz - 3 kHz), amplified and digitized (25 kHz) using TDT System 3 digital signal processors (Tucker Davis Technologies). BrainWare software (Tucker Davis Technologies) was used to control stimulus presentation and data acquisition and to extract action potential clusters for analysis in Matlab (The MathWorks).

All stimuli were pure tones of 50 ms (mapping stimuli) or 5 ms (conditioning stimuli) duration with 5-ms or 1-ms raised cosine onset and offset ramps, respectively. At the beginning of each experiment, 50-ms duration pure tones of varying frequency and level were used to measure response thresholds. For mapping of iso-intensity frequency tuning curves, nine stimuli were presented at a single supra-threshold level. Stimuli were presented 10 (mapping blocks immediately following a conditioning block) or 20 (all other mapping blocks) times in pseudorandom order in sweeps of 500 ms length. During the experiment response windows were chosen manually and, after inspection of the iso-intensity tuning curves, two frequencies were selected to construct conditioning pairs, a preferred (PF) and a non-preferred frequency (NPF). The former was chosen to lie at or close to the peak of the tuning curve, whereas the latter was chosen to lie outside the range of frequencies that the neuron strongly responded to (Fig. 1). During positive conditioning the first 5-ms stimulus in the conditioning pair was an NPF tone and the second a PF tone (Fig. 2). During negative conditioning that order was reversed. The interval between the onsets of the two stimuli in a pair was 8, 12, 16 or 30 ms, the rest period between two consecutive conditioning pairs was 100 ms and each conditioning block consisted of 600 pairs. Thus, a single block lasted

between ~68 s and 81 s. The experiment started with an initial preconditioning mapping block, followed by three alternating conditioning and mapping blocks. The NPF and PF as well as the conditioning interval remained constant for three consecutive conditioning blocks. In some cases one or two additional mapping blocks were presented to assess the persistence of tuning curve changes (Fig. 2). Single-tone conditioning experiments were carried out in identical manner as the pairing experiments, except that only one stimulus, either a NPF or PF tone, was presented.

Data analysis

Spike sorting was performed offline. Recordings were classed as either single units or small multi-unit clusters as judged from the quality of the spike shapes and the presence of a refractory period in the autocorrelation histogram. Spikes typically had a biphasic waveform, suggesting that we were recording from the region of the cell soma, rather than from axons.

For off-line analysis of frequency selectivity, spike trains from the pre- and post-conditioning mapping blocks were converted into post stimulus time histograms (PSTHs) with a 5 ms bin width (Fig. 1*A*). Most units, even in the awake animals, were dominated by onset responses, although additional, longer-latency components were frequently observed too. Because it has been reported that the frequency selectivity of the onset and offset components of A1 responses can vary (Qin et al., 2007), we focused here only on the onset response. The first bin of the PSTH to be included in this response window was the first bin to exceed the mean spontaneous firing rate, measured 250-500 ms after stimulus onset, by three standard deviations. The last bin to be included was that preceding the first bin in which the response fell to below 50% of the peak firing rate (Fig. 1*A*). The same response window was used for all pre- and post-conditioning mapping blocks for a given unit. Iso-intensity tuning curves were fitted with Gaussian functions to measure their best frequency (peak position), width (at half maximum) and peak firing rate (peak height).

To further analyze changes in the frequency representation, difference-tuning curves were generated by subtracting the pre-conditioning from the post-conditioning curves. In order to be able to average across many units, these were normalized by the maximum pre-conditioning firing rate, shifted and, if necessary, mirrored so that they could be aligned on the position of the NPF with the PF always lying on the left of the NPF. For the single-tone experiments the difference-tuning curves were aligned on the position of the conditioning tone, and tuning curves were, if necessary, mirrored to ensure that the unit's best frequency always lay to the left of the conditioning tone.

Cross-correlograms (*CCGs*) were obtained by calculating cross-correlations (C_{ab}) between spike trains recorded simultaneously at two different recording sites, a and b, normalizing the result and subtracting the shift predictor (Bair et al., 2001). Normalization involved dividing the cross-correlation by $\Theta(T)$, a triangular function representing the extent of overlap between the spike trains for each time lag T. This step corrects for the triangular shape of the cross-correlations caused by the fact that spike trains are finite duration data. A second normalization step involved division by the geometric mean spike rate ($\sqrt{(\lambda_a \lambda_b)}$). These two normalization steps changed the units of the CCG from a raw coincidence count to coincidences per spike. The same normalization was used for calculation of the shift predictor (SP). Shift predictors were computed based on the average cross-correlation between all non-simultaneous spike trains from sites a and b. The spike train CCG is given by the following equation:

$$CCG = \frac{C_{ab}}{\Theta(T)\sqrt{(\lambda_a \lambda_b)}} - SP$$

To quantify correlation strength we determined the peak of the smoothed (3 ms boxcar function) CCG, calculated the area under it and its width between the points to the left and the right of the peak at which the number of coincidences per spike fell below 3 standard deviations above the baseline correlation (measured between −100 ms and −75 ms and between 75 ms and 100 ms; see Fig. 10*A*). In addition, we also calculated the area under the CCG for a range of predefined widths from ±5 ms to ±50 ms. All analyses were carried out for all these measures of correlation strength but the outcomes tended to be very similar.

The cross-correlation functions used to assess spike timing precision during presentation of conditioning stimuli were 'all-way' cross-correlations between all the spike trains of a given unit recorded during positive conditioning and all the spike trains of the same unit recorded during negative conditioning using the same interval and conditioning stimuli. They were computed by simply cross-correlating the PSTHs.

Results

Recordings were made from a combination of small multi-unit clusters (n = 299) and single units (n = 94) in adult ferrets. All data presented here, apart from those in Fig. 5*D*, are from anesthetized animals.

Spike timing precision of conditioning responses

In this study, asynchronous presentation of pairs of conditioning stimuli, comprising one pure tone at the PF and a second at the NPF (Figs. 1 and 2), were repeatedly presented in an attempt to control the relative spike timing of different inputs to frequency-selective neurons in A1. In order to assess whether the conditioning stimuli can control the timing of neural activity in the auditory system in the intended manner, we analyzed spike trains recorded during the presentation of conditioning stimuli. Figure 3*A* shows PSTHs and spike rasters from a multi-unit cluster whose frequency tuning curve is depicted in Fig. 1*B*. They were obtained by presenting one positive and one negative conditioning block (Fig. 2*B*). The length of the onset asynchrony of the PF and NPF in each pair in these examples was 8 ms and is reflected in the interval between the peaks of the two PSTHs, which represent the response to the PF tone in each case. Thus, the peak occurs earlier during negative conditioning, in which the PF preceded the NPF, than it does during positive conditioning, when the order of the tones in each pair was reversed.

In order to quantify spike timing precision, we cross-correlated the spike trains obtained during positive and negative conditioning and measured the peak position and width of the resulting cross-correlation function (Fig. 3*B*). In this case, the peak occurred at 8 ms which, again, reflects the conditioning interval used, and its width at half maximum was 10 ms. A correspondence between conditioning interval and peak position in the cross-correlation function (Fig. 3*C*) was found for most of the recordings that could be assessed in this way, i.e. those units that underwent both positive and negative conditioning with the same interval length and tone frequencies. The mean cross-correlation width for this population was 29.27 ms (Fig. 3*D*), which is comparable to that reported during similar conditioning experiments in cat visual cortex (Fu et al., 2002)

Europe PMC Funders Author Manuscripts

Temporal specificity of frequency representation plasticity

The effects of asynchronous presentation of the conditioning stimuli on the frequency selectivity of A1 units was assessed by comparing iso-intensity tuning curves that were measured before and after each block of 600 conditioning pairs. STDP rules predict that positive conditioning should induce a strengthening of synapses from NPF-tuned neurons to PF-tuned neurons and shift the tuning curves of the latter towards the NPF, whereas negative conditioning should weaken synapses from NPF-tuned neurons to PF-tuned neurons and shift the tuning curves away from the NPF. Figure 4*A* shows a pre-conditioning tuning curve (black) and a post-conditioning tuning curve (red) derived by averaging responses from three mapping blocks that immediately followed each of three positive conditioning blocks. The conditioning stimuli used in this example had frequencies of 7.5 kHz (NPF) and 15.1 kHz (PF). Relative to the pre-conditioning tuning curve, and in line with STDP predictions, the post-conditioning tuning curve is shifted slightly towards the NPF.

In order to quantify the effects of the conditioning procedure on iso-intensity tuning curve position and shape, Gaussian functions were fitted. From these fits, the best frequency (peak of the fitted function), tuning width (at half height) and peak firing rate of the tuning curves were derived. The best sound frequencies of the tuning curves are indicated by short vertical lines above each curve. Thus, in Fig. 4*A*, the best frequency shifted down in value towards the NPF. Another example of positive conditioning, this time using an NPF that was on the high-frequency edge of the iso-intensity tuning curve, is shown in Fig. 4*C*. Here the best frequency shifted slightly up in value. By contrast, Figs. 4*B* and *D* show examples of negative conditioning, in which the best sound frequencies shifted away from the NPF.

Shifts were quantified as the difference between the best frequencies of the pre- and post-conditioning iso-intensity tuning curves and normalized by the pre-conditioning tuning width. Positive conditioning with an 8 ms interval induced a significant shift of the tuning curves towards the NPF by, on average, 1.71±0.48% (mean±standard error of the mean, $p < 0.0005$, t-test, n = 183). Negative conditioning induced a shift in the opposite direction, away from the NPF, by −2.22±0.47% ($p < 0.0005$, n = 165). This fulfils the order specificity of our predictions. If the underlying mechanism of this effect is dependent on STDP of neural connections, such a shift should not occur with longer conditioning intervals. This was confirmed in our data. Although similar shifts still occurred with 12 ms intervals (positive conditioning: 1.92±0.77%, $p < 0.05$, n = 129; negative conditioning: −2.06±0.98%, $p < 0.05$, n = 108), no such effect was observed with 16 or 30 ms intervals (Fig. 5*A*).

Figure 5*B* shows changes in tuning width and firing rate as a function of the conditioning interval. Conditioning induced a widening of frequency tuning with the shorter intervals of 8, 12 and 16 ms, but there were no significant differences between positive and negative conditioning at any of the intervals ($p > 0.46$). Firing rates were not affected by conditioning in any systematic way and there were no differences in firing rate changes between negative and positive conditioning at any of the intervals ($p > 0.2$). We examined separately our population of single units (n = 94), which showed very similar temporal specificity in their best frequency shifts, with a significant difference between positive and negative conditioning shifts for 8 ms intervals ($p < 0.0005$) (Fig. 5*C*), to that observed for the entire sample (Fig. 5*A*). Consequently, the single units were combined with the multi-unit responses for all analyses.

We also examined the effect of conditioning on frequency selectivity in A1 of two alert, head-restrained ferrets (see Materials and Methods for details). The experimental procedure and analysis were identical. However, recordings were made with tungsten-in-glass electrodes, stimuli were presented through a single free-field speaker placed in front of the animal and only two intervals (8 and 30 ms) were tested. Equivalent shifts in best sound

frequency were observed in the awake animals to those measured under anesthesia, with a significant difference between positive and negative conditioning at the 8 ms interval ($p < 0.005$), but not at 30 ms (Fig. 5*D*).

Profile of tuning curve changes

To find out whether the changes in best frequency were brought about through changes specific to either the NPF or PF or to changes beyond the stimulated frequencies, the data were further analyzed in terms of difference-tuning curves by subtracting the pre-conditioning from the post-conditioning tuning curves. After normalizing, shifting and, if necessary, mirroring the difference-tuning curves, they were aligned on the NPF and averaged across all units that underwent positive or negative conditioning with 8 or 12 ms intervals. Positive conditioning resulted in a potentiation of the response at the NPF and at nearby frequencies, no change at the PF and compensatory depression on the opposite side of the tuning curve. Negative conditioning resulted in the opposite pattern of changes, i.e. depression around the NPF, no change at the PF and compensatory potentiation on the far side (Fig. 6*A*).

Single-tone conditioning

In order to determine whether changes in best frequency were specific to conditioning with pairs of tones that differed in frequency, we also examined the effect of repeatedly presenting a single tone frequency either at or close to the peak of the tuning curve (PF) or outside the range of frequencies to which the neuron responded strongly to (NPF). However, neither NPF-alone nor PF-alone conditioning produced significant shifts in best frequency (NPF: −0.54±0.88%, $p > 0.5$, n = 141; PF: 0.49±1.01%, n = 92, $p > 0.5$). Inspection of the difference tuning curves revealed a general increase in responsiveness at most sound frequencies (Fig. 6*B,C*), in contrast to the order-specific changes observed when two different tone frequencies were used.

Time scales of induction and persistence of plasticity

To examine stimulus-timing-dependent plasticity of best frequency in more detail, we pooled data from those conditions that produced significant effects, i.e. the 8 ms and 12 ms intervals between the stimuli in each conditioning pair, and reversed the sign of the shifts from negative conditioning, so that results could be plotted as shifts in the ‘predicted direction’.

In order to assess the time scale over which best frequency shifts occur, the tuning curves obtained after each of the three conditioning blocks were analyzed separately. Figure 4*C* shows a pre-conditioning tuning curve and one tuning function per mapping block immediately following each of three positive conditioning blocks. The largest shift in best frequency, in this case toward the NPF, was observed after the third conditioning block. Figure 4*D* shows a similar example for negative conditioning. For this unit, the best frequency gradually shifted away from the NPF as the amount of conditioning was increased. The population average shows a similar picture to these examples (Fig. 7*A*). The maximum shift was observed immediately after the last of the three conditioning blocks. Nevertheless, one conditioning block of 600 tone pairs, representing little more than one minute of conditioning, was sufficient to produce a significant effect.

In several experiments an additional mapping block was included after a delay of ~6 minutes following the last conditioning block. Two examples are depicted in Fig. 4*B* and *C* by the light green tuning curves. In the former example, the best frequency of the unit had shifted back slightly in the direction of its original value, whereas in the latter example the best frequency remained at its new value after this delay. A sixth mapping block sometimes

followed ~12 minutes after the last conditioning block, an example of which is shown in dark green in Fig. 4*B*. This revealed that the best frequency of the unit had shifted back further and even overshot its original pre-conditioning value. On average, significant best frequency shifts persisted throughout the fifth mapping block (Fig. 7*B*), but had disappeared by the sixth block (Fig. 7*C*). The transient nature of the alterations in best frequency, coupled with their systematic dependence upon the interval between and order in which the conditioning stimuli were presented, rule out any possibility that the observed effects were due to a drift in unit responsiveness over time.

Factors affecting plasticity: frequency separation of conditioning stimuli

The frequency difference between two stimuli in a conditioning pair was varied from experiment to experiment and spanned a range of 2.1 octaves. It was predicted that conditioning stimuli comprising tones that are widely separated in frequency would produce smaller changes in frequency tuning, presumably because they recruit populations of neurons that are only sparsely connected. Plotting shifts as a function of the frequency difference between the stimuli in a conditioning pair revealed that differences of ~1 octave or less were, indeed, more effective than larger ones (Fig. 8*A*). At what point the frequency difference becomes too small and plasticity decreases because both conditioning stimuli activate the same population of neurons is, however, unclear from these data.

Factors affecting plasticity: cortical depth

All experiments on anesthetized animals were carried out using 16-site single-shank silicon probes (Fig. 8*B*). Care was taken to insert these electrodes at an angle that was perpendicular to the cortical surface, leaving the most proximal recording site just above the surface, so that depth measurements could be related to the cortical layers. Hardly any recordings were obtained on the deepest sites and these were therefore excluded from this analysis. By plotting the shifts in best frequency produced by conditioning as a function of recording depth, it is clear that significant shifts occurred only for a restricted range of electrode sites in the upper cortical layers (Fig. 8*C*).

Because it was not possible to pass current through the single-shank silicon probes in order to mark the recording sites with electrolytic lesions, six measurements of the thickness of the cortical layers were made in each of two different ferrets using coronal and horizontal sections of the brain that had been stained either for Nissl substance or with the NeuN antibody. These measurements were made in different regions of the MEG, so that the full range of electrode positions in A1 was covered (see inset in Fig. 8*C*). Not surprisingly, they revealed that the thickness of each layer varied to some extent with location over the MEG and with the size of the animal. The upper and lower borders of each layer measured at the thinnest (left) and thickest (right) of those six positions are therefore indicated by colored bars on either side of the graph in Fig. 8*C*, respectively. Any differences in the angle of the recording electrodes or the plane of cutting of the sections used to make these measurements will add to the variation in the estimated range of values. Nevertheless, Fig. 8*C* suggests that repeated pairing of two tones of different frequencies induces significant shifts in A1 frequency selectivity only in layers II/III and in layer IV.

Factors not affecting plasticity: tuning width, rate and temporal precision of responses

Neither the tuning curve width (Fig. 9*A*) nor the number of spikes fired during conditioning (Fig. 9*B*) appeared to influence the magnitude of the shifts in best frequency. We also looked at the temporal precision (as described in Fig. 3) of A1 responses. However, no relationship could be found between the magnitude of the shift and either the difference between the interval between the conditioning tone pairs and the peak of the cross-correlation function (Fig. 9C) or the width of the function (Fig. 9*D*).

Inter-neuronal correlation

Repeated asynchronous conditioning of two adjacent retinal areas has been reported to cause changes in inter-neuronal correlation between the responses of neurons in the primary visual cortex (V1) of cats with similar receptive fields, which was attributed to conditioning-induced changes in common input (Fu et al., 2002). We therefore examined whether similar changes in inter-neuronal correlation were brought about by our conditioning procedure. To test for changes in correlation strength, we computed cross-correlograms (CCGs, see Materials and Methods for details) between pairs of recordings from neurons with similar frequency selectivity. The configuration of the recording probes that we used allowed us to measure inter-neuronal correlation at different cortical depths and at varying amounts of inter-neuronal separation.

Figure 10*A* illustrates CCGs obtained by correlating neuronal activity from a fairly superficial recording site with activity from progressively deeper recording sites. Not surprisingly, correlation strength decreased as the distance between the units increased. In order to quantify correlation strength, one can measure the height of the peak of the CCG, its width or the area under it. Figure 10*B* plots the average CCG peak height as a function of recording site combination. The warmer colors clearly show that the correlation strength is greatest for nearby units. Potential changes in correlation strength brought about by conditioning were assessed by subtracting post-from pre-conditioning correlation strength and normalizing this difference score by the pre-conditioning correlation strength. Figure 10*C* shows how the correlation strength, expressed as either the width or peak height of the CCG, changed as a function of conditioning interval for recording sites separated by up to 0.3 mm. Fu et al. (2002) found that asynchronous pairing of visual stimuli at neighboring spatial locations altered the cross-correlation between the spike trains of simultaneously-recorded neurons in cat V1 and shifted their receptive fields in a manner that depended upon the interval between and order in which the stimuli were presented. Significant changes in correlation strength were also observed in A1 at certain conditioning intervals ($p < 0.05$). However, despite assessing a range of inter-site distances and cortical depths, we could find no evidence that these changes followed the same temporal pattern (Fig. 10*C*) to that observed for the shifts in auditory frequency tuning (Fig. 5).

Discussion

We showed that repeated, asynchronous pairing of tones of different frequencies can alter sound frequency selectivity in A1 in a manner consistent with the key features of STDP. Significant changes occurred when the onset asynchrony of tone pairs was 8 or 12 ms, but not with longer intervals, and the direction of change depended upon the order of stimulation. By contrast, shifts in best frequency did not occur following repeated presentation of a single tone frequency. As in previous studies of stimulus-timing-dependent plasticity, these receptive-field modifications were observed under anesthesia. Importantly, however, similar shifts were also observed in alert ferrets.

Profile of tuning curve changes

The changes in best frequency were brought about through a combination of potentiation (positive conditioning) or depression (negative conditioning) at the NPF and neighboring frequencies, accompanied by compensatory depression (positive conditioning) or potentiation (negative conditioning) on the far side of the tuning curves. Similar spread of plasticity has been reported with STDP of whisker-evoked responses (Jacob et al., 2007) and visual receptive fields (Meliza and Dan, 2006; Vislay-Meltzer et al., 2006), and may reflect the distribution of neurons activated by a given stimulus or the spread of LTP/LTD to neighboring synapses (Engert and Bonhoeffer, 1997; Fitzsimonds et al., 1997).

Compensatory changes similar to those observed here also occur with other forms of cortical frequency plasticity (e.g.Bakin and Weinberger, 1996) and could be related to homeostatic mechanisms that produce heterosynaptic changes opposite in sign to the LTP/LTD at the stimulated site (Scanziani et al., 1996; Royer and Pare, 2003).

Stability of plasticity

The duration of stimulus-timing-dependent plasticity in A1 is similar to that reported in V1 of pentothal-anesthetized cats (Yao and Dan, 2001) and for STDP in barrel cortex of urethane-anesthetized rats (Jacob et al., 2007), suggesting that the inclusion of ketamine in our anesthetic protocol did not limit the persistence of the effect. The short duration of this plasticity is likely due to neuronal activity in the intact brain, which makes it harder to establish stable and long-lasting synaptic modifications (review by Zhou and Poo, 2004). Thus, LTP and LTD at retinotectal synapses in *Xenopus* tadpoles can be rapidly reversed if the neurons are allowed to fire spontaneously for a few minutes (Zhou et al., 2003), and otherwise long-lasting spike-timing-induced receptive field shifts in these cells can be reversed by 10 minutes of spiking in response to random visual stimulation (Vislay-Meltzer et al., 2006). These effects of neuronal activity, together with the weaker control over spiking that sensory stimuli provide compared to direct current injections, could further explain the relatively large number of stimulus pairings required to produce stimulus-timing-dependent plasticity *in vivo*.

Potential origins of plasticity

Stimulus-timing-dependent plasticity in orientation tuning in V1 exhibits inter-ocular transfer, suggesting that the underlying changes take place within the cortex itself (Schuett et al., 2001; Yao et al., 2004). By contrast, plasticity in the spatial selectivity of V1 neurons or in the frequency selectivity of A1 neurons, which are properties of the receptor cells, could potentially arise at lower levels. Shifts in cortical frequency tuning are largely restricted to cortical layers II/III and IV. This resembles the laminar specificity of receptive field plasticity induced in A1 by pairing tones of different frequencies with simultaneous current injections, which was most prevalent in layer IV and upper layer V (Cruikshank and Weinberger, 1996). Layers III and IV are innervated by the ventral division of the medial geniculate body (Winer et al., 2005) and functional connections appear to be limited to within one-third of an octave of the cortical best frequency (Miller et al., 2001). This is consistent with our finding that the magnitude of auditory stimulus-timing-dependent plasticity declined significantly when the frequency difference between the conditioning tones exceeded half an octave, implying that plasticity could be present in thalamocortical inputs.

According to Schuett et al. (2001), stimulus-timing-dependent plasticity of orientation tuning in V1 also varies with cortical depth. They observed significant changes in layers II/III and V/VI but not layer IV. This could reflect an age difference, as these authors recorded from kittens. Nevertheless, they interpreted the laminar specificity and inter-ocular transfer of orientation preference shifts as evidence for the involvement of cortico-cortical synapses outside layer IV. Fu et al. (2002) reached the same conclusion after finding that conditioning-induced shifts in receptive field position in adult cat V1 were accompanied by changes in cross-correlated activity of simultaneously-recorded cortical neuron pairs.

A1 receives extensive cortico-cortical inputs (Rouiller et al., 1991; Kaas and Hackett, 2000; Lee and Winer, 2008), which are thought to terminate mostly within layers III and IV (Winer, 1992), where we observed the largest receptive field shifts. Intra-cortical inputs are responsible for sub-threshold receptive fields (Kaur et al., 2004; Liu et al., 2007), which could provide a basis for plasticity of frequency tuning. However, if cortical synapses are

directly involved in the plasticity leading to alterations in frequency selectivity, we might expect to observe larger shifts in neurons whose firing was more tightly controlled by the conditioning stimuli. This was not the case, possibly because changes expressed in the cortex are mediated by a subgroup of neurons that responded to the conditioning stimuli with reliable and temporally precise spiking, which then influence the tuning of other neurons in the cortical network. Alternatively, the relevant changes in synaptic strength and frequency tuning could originate subcortically and then be inherited by the auditory cortex. Either way, these findings highlight the fact that while the temporal specificity of stimulus-timing-dependent plasticity resembles that of STDP, the site of origin of these effects as well as their underlying synaptic mechanisms remain to be determined.

Our finding that stimulus-timing-dependent plasticity in the representation of sound frequency in A1 is greatest in the upper cortical layers is supported by other studies. LTP and LTD can be induced in layer IV in cortical slices from young animals, whereas plasticity seems to be restricted to layers II/III in adults (Crair and Malenka, 1995; Dudek and Friedlander, 1996; Feldman et al., 1998). This fits with developmental changes in the laminar distribution of NMDAR1 immunostaining in both ferret and cat V1, with high levels persisting into adulthood only in layers II/III (Catalano et al., 1997). It may seem surprising that plasticity in the superficial cortical layers is not communicated to the deeper layers. However, the receptive field properties of neurons in the infragranular layers differ from those found more superficially and their response latencies can be shorter (Sugimoto et al., 1997; Kral et al., 2000; Wallace and Palmer, 2008). This indicates that they receive inputs from other sources, including the thalamus (Mitani and Shimokouchi, 1985; Prieto et al., 1994). Moreover, slice recordings have revealed that layer V neurons possess higher spiking thresholds than those in layers II/II, which could provide a potential mechanism whereby the former acts as a barrier preventing information/plasticity from spreading beyond the superficial layers (Atzori et al., 2004; Nichols et al., 2007).

Future challenges

STDP has been demonstrated in cochlear nucleus slices (Tzounopoulos et al., 2004), but it remains to be seen whether it occurs in the auditory system under natural conditions, how it shapes the developing system, and what role it might play in a mature system undergoing refinement and learning. STDP has been implicated in the cortical plasticity that follows whisker trimming or focal retinal lesions (Young et al., 2007) and is therefore presumably involved in the reorganization of cortical tonotopicity produced by partial cochlear lesions (Kamke et al., 2005). Moreover, STDP has been proposed as a mechanism underlying certain forms of auditory perceptual learning (Mossbridge et al., 2006), an idea supported by the finding that asynchronous conditioning in the visual system affects perception in an STDP-like manner (Yao and Dan, 2001; Fu et al., 2002). Our own unpublished observations suggest that asynchronous stimulus presentation can alter the sensitivity of human listeners to binaural localization cues in a similar fashion. Although no behavioral experiments were carried out in the present study, training can alter frequency discrimination thresholds (Recanzone et al., 1993; Irvine and Wright, 2005), implying that sound frequency perception is also likely to be influenced by stimulus-timing-dependent plasticity.

Modulations in frequency content are a common feature of natural sounds, including animal vocalizations, and could be well suited to induce the neuronal activity patterns required for STDP. Interestingly, repeated exposure to vocalizations in a behaviorally-relevant context alters the temporal pattern codes through which these sounds could be represented in A1 (Schnupp et al., 2006). Although it is not known whether STDP contributes to the emergence of sensitivity to natural sounds, it has been implicated in the development of direction selectivity in the visual system (Engert et al., 2002; Mu and Poo, 2006). Furthermore, STDP can account for both the shifts in V1 receptive fields and the perceptual

illusions induced by adaptation to moving gratings (Fu et al., 2004), as well as the changes reported in hippocampal place fields (Mehta et al., 2000; Lee et al., 2004) and thalamic head-direction tuning curves (Yu et al., 2006) following animal locomotion, and could underlie whisker-pairing-induced changes in barrel cortex (Delacour et al., 1987). The use of more complex stimuli should therefore help to reveal the importance of this phenomenon in shaping auditory function.

Acknowledgments

Our work is funded by the Wellcome Trust through a four-year studentship to JC Dahmen, a Clinical Scientist Fellowship to DEH Hartley and a Principal Research Fellowship to AJ King. We thank Bashir Ahmed, Fernando Nodal, and Kerry Walker for help with surgery and data collection and Victoria Bajo for providing us with estimates of the thickness of the cortical layers.

References

Atzori M, Flores Hernandez J, Pineda JC. Interlaminar differences of spike activation threshold in the auditory cortex of the rat. Hear Res. 2004; 189:101–106. [PubMed: 14987757]

Bair W, Zohary E, Newsome WT. Correlated firing in macaque visual area MT: time scales and relationship to behavior. J Neurosci. 2001; 21:1676–1697. [PubMed: 11222658]

Bakin JS, Weinberger NM. Induction of a physiological memory in the cerebral cortex by stimulation of the nucleus basalis. Proc Natl Acad Sci U S A. 1996; 93:11219–11224. [PubMed: 8855336]

Bao S, Chan VT, Merzenich MM. Cortical remodelling induced by activity of ventral tegmental dopamine neurons. Nature. 2001; 412:79–83. [PubMed: 11452310]

Blake DT, Heiser MA, Caywood M, Merzenich MM. Experience-dependent adult cortical plasticity requires cognitive association between sensation and reward. Neuron. 2006; 52:371–381. [PubMed: 17046698]

Caporale N, Dan Y. Spike timing-dependent plasticity: a Hebbian learning rule. Annu Rev Neurosci. 2008; 31:25–46. [PubMed: 18275283]

Catalano SM, Chang CK, Shatz CJ. Activity-dependent regulation of NMDAR1 immunoreactivity in the developing visual cortex. J Neurosci. 1997; 17:8376–8390. [PubMed: 9334411]

Celikel T, Szostak VA, Feldman DE. Modulation of spike timing by sensory deprivation during induction of cortical map plasticity. Nat Neurosci. 2004; 7:534–541. [PubMed: 15064767]

Cheung SW, Nagarajan SS, Schreiner CE, Bedenbaugh PH, Wong A. Plasticity in primary auditory cortex of monkeys with altered vocal production. J Neurosci. 2005; 25:2490–2503. [PubMed: 15758157]

Crair MC, Malenka RC. A critical period for long-term potentiation at thalamocortical synapses. Nature. 1995; 375:325–328. [PubMed: 7753197]

Cruikshank SJ, Weinberger NM. Receptive-field plasticity in the adult auditory cortex induced by Hebbian covariance. J Neurosci. 1996; 16:861–875. [PubMed: 8551366]

Dahmen JC, King AJ. Learning to hear: plasticity of auditory cortical processing. Curr Opin Neurobiol. 2007; 17:456–464. [PubMed: 17714932]

de Villers-Sidani E, Chang EF, Bao S, Merzenich MM. Critical period window for spectral tuning defined in the primary auditory cortex (A1) in the rat. J Neurosci. 2007; 27:180–189. [PubMed: 17202485]

Delacour J, Houcine O, Talbi B. “Learned” changes in the responses of the rat barrel field neurons. Neuroscience. 1987; 23:63–71. [PubMed: 3683870]

Dudek SM, Friedlander MJ. Developmental down-regulation of LTD in cortical layer IV and its independence of modulation by inhibition. Neuron. 1996; 16:1097–1106. [PubMed: 8663986]

Engert F, Bonhoeffer T. Synapse specificity of long-term potentiation breaks down at short distances. Nature. 1997; 388:279–284. [PubMed: 9230437]

Engert F, Tao HW, Zhang LI, Poo MM. Moving visual stimuli rapidly induce direction sensitivity of developing tectal neurons. Nature. 2002; 419:470–475. [PubMed: 12368854]

Europe PMC Funders Author Manuscripts

Feldman DE, Nicoll RA, Malenka RC, Isaac JT. Long-term depression at thalamocortical synapses in developing rat somatosensory cortex. Neuron. 1998; 21:347–357. [PubMed: 9728916]

Fitzsimonds RM, Song HJ, Poo MM. Propagation of activity-dependent synaptic depression in simple neural networks. Nature. 1997; 388:439–448. [PubMed: 9242402]

Fritz J, Shamma S, Elhilali M, Klein D. Rapid task-related plasticity of spectrotemporal receptive fields in primary auditory cortex. Nat Neurosci. 2003; 6:1216–1223. [PubMed: 14583754]

Froemke RC, Merzenich MM, Schreiner CE. A synaptic memory trace for cortical receptive field plasticity. Nature. 2007; 450:425–429. [PubMed: 18004384]

Fu YX, Shen Y, Gao H, Dan Y. Asymmetry in visual cortical circuits underlying motion-induced perceptual mislocalization. J Neurosci. 2004; 24:2165–2171. [PubMed: 14999067]

Fu YX, Djupsund K, Gao H, Hayden B, Shen K, Dan Y. Temporal specificity in the cortical plasticity of visual space representation. Science. 2002; 296:1999–2003. [PubMed: 12065829]

Irvine DR, Wright BA. Plasticity of spectral processing. Int Rev Neurobiol. 2005; 70:435–472. [PubMed: 16472642]

Jacob V, Brasier DJ, Erchova I, Feldman D, Shulz DE. Spike timing-dependent synaptic depression in the in vivo barrel cortex of the rat. J Neurosci. 2007; 27:1271–1284. [PubMed: 17287502]

Kaas JH, Hackett TA. Subdivisions of auditory cortex and processing streams in primates. Proc Natl Acad Sci U S A. 2000; 97:11793–11799. [PubMed: 11050211]

Kamke MR, Brown M, Irvine DR. Basal forebrain cholinergic input is not essential for lesion-induced plasticity in mature auditory cortex. Neuron. 2005; 48:675–686. [PubMed: 16301182]

Kaur S, Lazar R, Metherate R. Intracortical pathways determine breadth of subthreshold frequency receptive fields in primary auditory cortex. J Neurophysiol. 2004; 91:2551–2567. [PubMed: 14749307]

Kilgard MP, Merzenich MM. Cortical map reorganization enabled by nucleus basalis activity. Science. 1998; 279:1714–1718. [PubMed: 9497289]

King AJ, Hutchings ME, Moore DR, Blakemore C. Developmental plasticity in the visual and auditory representations in the mammalian superior colliculus. Nature. 1988; 332:73–76. [PubMed: 3347247]

Knudsen EI, Brainard MS. Visual instruction of the neural map of auditory space in the developing optic tectum. Science. 1991; 253:85–87. [PubMed: 2063209]

Kral A, Hartmann R, Tillein J, Heid S, Klinke R. Congenital auditory deprivation reduces synaptic activity within the auditory cortex in a layer-specific manner. Cereb Cortex. 2000; 10:714–726. [PubMed: 10906318]

Lee CC, Winer JA. Connections of cat auditory cortex: III. Corticocortical system. J Comp Neurol. 2008; 507:1920–1943. [PubMed: 18271030]

Lee I, Rao G, Knierim JJ. A double dissociation between hippocampal subfields: differential time course of CA3 and CA1 place cells for processing changed environments. Neuron. 2004; 42:803–815. [PubMed: 15182719]

Liu BH, Wu GK, Arbuckle R, Tao HW, Zhang LI. Defining cortical frequency tuning with recurrent excitatory circuitry. Nat Neurosci. 2007; 10:1594–1600. [PubMed: 17994013]

Manunta Y, Edeline JM. Noradrenergic induction of selective plasticity in the frequency tuning of auditory cortex neurons. J Neurophysiol. 2004; 92:1445–1463. [PubMed: 15084638]

Markram H, Lubke J, Frotscher M, Sakmann B. Regulation of synaptic efficacy by coincidence of postsynaptic APs and EPSPs. Science. 1997; 275:213–215. [PubMed: 8985014]

Mehta MR, Quirk MC, Wilson MA. Experience-dependent asymmetric shape of hippocampal receptive fields. Neuron. 2000; 25:707–715. [PubMed: 10774737]

Meliza CD, Dan Y. Receptive-field modification in rat visual cortex induced by paired visual stimulation and single-cell spiking. Neuron. 2006; 49:183–189. [PubMed: 16423693]

Miller LM, Escabi MA, Read HL, Schreiner CE. Functional convergence of response properties in the auditory thalamocortical system. Neuron. 2001; 32:151–160. [PubMed: 11604146]

Mitani A, Shimokouchi M. Neuronal connections in the primary auditory cortex: an electrophysiological study in the cat. J Comp Neurol. 1985; 235:417–429. [PubMed: 2987316]

Mossbridge JA, Fitzgerald MB, O'Connor ES, Wright BA. Perceptual-learning evidence for separate processing of asynchrony and order tasks. J Neurosci. 2006; 26:12708–12716. [PubMed: 17151274]

Mu Y, Poo MM. Spike timing-dependent LTP/LTD mediates visual experience-dependent plasticity in a developing retinotectal system. Neuron. 2006; 50:115–125. [PubMed: 16600860]

Nichols JA, Jakkamsetti VP, Salgado H, Dinh L, Kilgard MP, Atzori M. Environmental enrichment selectively increases glutamatergic responses in layer II/III of the auditory cortex of the rat. Neuroscience. 2007; 145:832–840. [PubMed: 17291690]

Norena AJ, Gourevitch B, Aizawa N, Eggermont JJ. Spectrally enhanced acoustic environment disrupts frequency representation in cat auditory cortex. Nat Neurosci. 2006; 9:932–939. [PubMed: 16783369]

Ohl FW, Scheich H, Freeman WJ. Change in pattern of ongoing cortical activity with auditory category learning. Nature. 2001; 412:733–736. [PubMed: 11507640]

Polley DB, Steinberg EE, Merzenich MM. Perceptual learning directs auditory cortical map reorganization through top-down influences. J Neurosci. 2006; 26:4970–4982. [PubMed: 16672673]

Prieto JJ, Peterson BA, Winer JA. Morphology and spatial distribution of GABAergic neurons in cat primary auditory cortex (AI). J Comp Neurol. 1994; 344:349–382. [PubMed: 7914896]

Qin L, Chimoto S, Sakai M, Wang J, Sato Y. Comparison between offset and onset responses of primary auditory cortex ON-OFF neurons in awake cats. J Neurophysiol. 2007; 97:3421–3431. [PubMed: 17360820]

Recanzone GH, Schreiner CE, Merzenich MM. Plasticity in the frequency representation of primary auditory cortex following discrimination training in adult owl monkeys. J Neurosci. 1993; 13:87–103. [PubMed: 8423485]

Rouiller EM, Simm GM, Villa AE, de Ribaupierre Y, de Ribaupierre F. Auditory corticocortical interconnections in the cat: evidence for parallel and hierarchical arrangement of the auditory cortical areas. Exp Brain Res. 1991; 86:483–505. [PubMed: 1722171]

Royer S, Pare D. Conservation of total synaptic weight through balanced synaptic depression and potentiation. Nature. 2003; 422:518–522. [PubMed: 12673250]

Scanziani M, Malenka RC, Nicoll RA. Role of intercellular interactions in heterosynaptic long-term depression. Nature. 1996; 380:446–450. [PubMed: 8602244]

Schnupp JW, Hall TM, Kokelaar RF, Ahmed B. Plasticity of temporal pattern codes for vocalization stimuli in primary auditory cortex. J Neurosci. 2006; 26:4785–4795. [PubMed: 16672651]

Schuett S, Bonhoeffer T, Hubener M. Pairing-induced changes of orientation maps in cat visual cortex. Neuron. 2001; 32:325–337. [PubMed: 11684001]

Sugimoto S, Sakurada M, Horikawa J, Taniguchi I. The columnar and layer-specific response properties of neurons in the primary auditory cortex of Mongolian gerbils. Hear Res. 1997; 112:175–185. [PubMed: 9367240]

Tzounopoulos T, Kim Y, Oertel D, Trussell LO. Cell-specific, spike timing-dependent plasticities in the dorsal cochlear nucleus. Nat Neurosci. 2004; 7:719–725. [PubMed: 15208632]

Vislay-Meltzer RL, Kampff AR, Engert F. Spatiotemporal specificity of neuronal activity directs the modification of receptive fields in the developing retinotectal system. Neuron. 2006; 50:101–114. [PubMed: 16600859]

Wallace MN, Palmer AR. Laminar differences in the response properties of cells in the primary auditory cortex. Exp Brain Res. 2008; 184:179–191. [PubMed: 17828392]

Winer, JA. The Functional Architecture of the Medial Geniculate Body and the Primary Auditory Cortex. In: Popper, AN.; Fay, RR.; Webster, DE., editors. The Mammalian Auditory Pathway: Neuroanatomy. Springer; New York: 1992. p. 222-409.

Winer JA, Miller LM, Lee CC, Schreiner CE. Auditory thalamocortical transformation: structure and function. Trends Neurosci. 2005; 28:255–263. [PubMed: 15866200]

Wolters A, Sandbrink F, Schlottmann A, Kunesch E, Stefan K, Cohen LG, Benecke R, Classen J. A temporally asymmetric Hebbian rule governing plasticity in the human motor cortex. J Neurophysiol. 2003; 89:2339–2345. [PubMed: 12612033]

Wolters A, Schmidt A, Schramm A, Zeller D, Naumann M, Kunesch E, Benecke R, Reiners K, Classen J. Timing-dependent plasticity in human primary somatosensory cortex. J Physiol. 2005; 565:1039–1052. [PubMed: 15845584]

Yao H, Dan Y. Stimulus timing-dependent plasticity in cortical processing of orientation. Neuron. 2001; 32:315–323. [PubMed: 11684000]

Yao H, Shen Y, Dan Y. Intracortical mechanism of stimulus-timing-dependent plasticity in visual cortical orientation tuning. Proc Natl Acad Sci U S A. 2004; 101:5081–5086. [PubMed: 15044699]

Young JM, Waleszczyk WJ, Wang C, Calford MB, Dreher B, Obermayer K. Cortical reorganization consistent with spike timing-but not correlation-dependent plasticity. Nat Neurosci. 2007; 10:887–895. [PubMed: 17529985]

Yu X, Yoganarasimha D, Knierim JJ. Backward shift of head direction tuning curves of the anterior thalamus: comparison with CA1 place fields. Neuron. 2006; 52:717–729. [PubMed: 17114054]

Zhang LI, Bao S, Merzenich MM. Persistent and specific influences of early acoustic environments on primary auditory cortex. Nat Neurosci. 2001; 4:1123–1130. [PubMed: 11687817]

Zhang LI, Tao HW, Holt CE, Harris WA, Poo M. A critical window for cooperation and competition among developing retinotectal synapses. Nature. 1998; 395:37–44. [PubMed: 9738497]

Zhou Q, Poo MM. Reversal and consolidation of activity-induced synaptic modifications. Trends Neurosci. 2004; 27:378–383. [PubMed: 15219736]

Zhou Q, Tao HW, Poo MM. Reversal and stabilization of synaptic modifications in a developing visual system. Science. 2003; 300:1953–1957. [PubMed: 12817152]

Europe PMC Funders Author Manuscripts

Europe PMC Funders Author Manuscripts

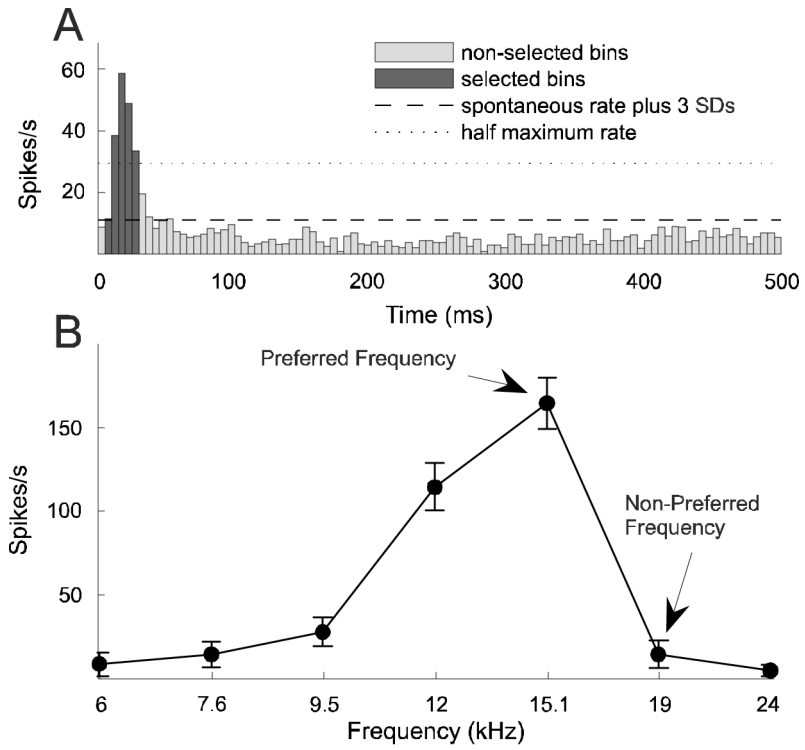

Figure 1.

Determination of response window and conditioning stimuli. ***A***, An average post stimulus time histogram (PSTH, 5 ms resolution) was generated for each unit by averaging its responses over all mapping blocks and sweeps in order to determine its onset response window. Iso-intensity tuning curves, such as the pre-conditioning tuning curve in ***B***, were based on the firing rates measured during this response window (dark bars), which included bins extending from the first one to exceed the spontaneous firing rate (measured 250-500 ms after stimulus onset) by at least 3 standard deviations (SDs) to the one preceding the first bin after the response fell to below 50% of the peak firing rate. Two frequencies were selected from the iso-intensity tuning curve to construct conditioning pairs, a preferred frequency (PF) and a non-preferred (NPF) one. The former had to lie within the range of frequencies to which the unit responded strongly, the latter outside of that range.

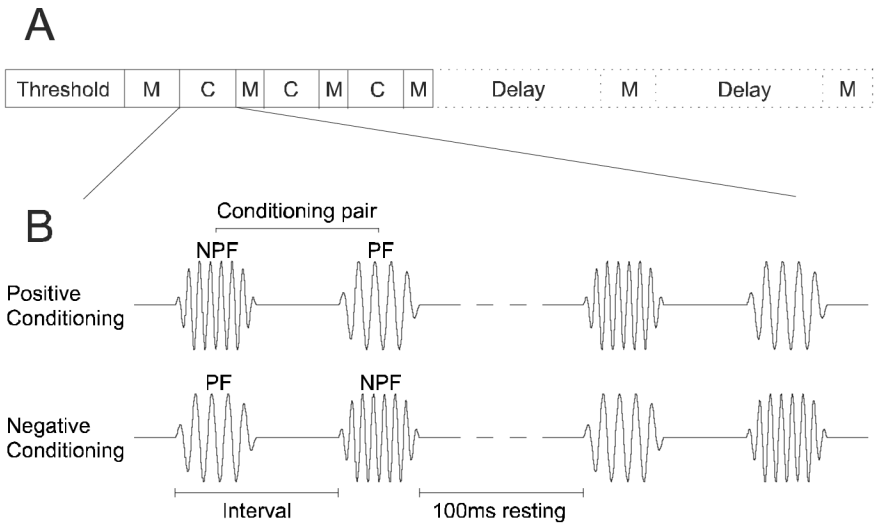

Figure 2.

Experimental procedure and conditioning stimuli. ***A***, After determining unit threshold at each recording site, an iso-intensity tuning curve was obtained in an initial preconditioning mapping (M) block, which was followed by three alternating conditioning (C) and mapping blocks. In some cases, one or two additional mapping blocks were included after a delay, in order to probe the persistence of any changes in frequency tuning. ***B***, Pairs of conditioning stimuli comprised two 5-ms pure tones of different frequencies (see Fig. 1). During positive conditioning the non-preferred frequency tone (NPF) preceded the preferred frequency tone (PF). During negative conditioning the order was reversed. The interval between the onsets of the two stimuli in a pair was either 8, 12, 16 or 30 ms, and the rest period between two consecutive pairs was fixed at 100 ms. Conditioning pairs were presented in blocks of 600.

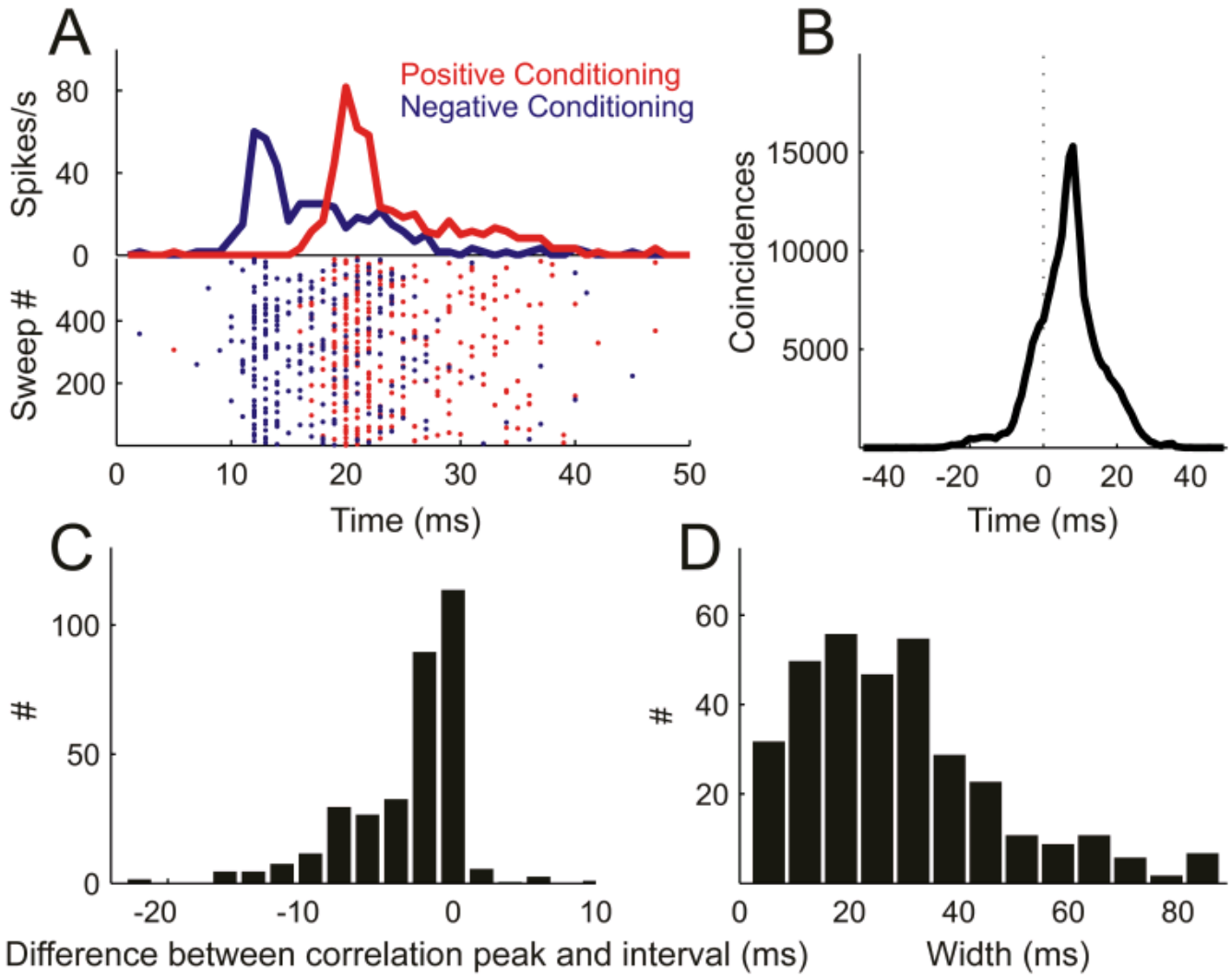

Figure 3.

Spike timing precision of conditioning responses. ***A***, Raster plots (lower) and PSTHs (upper) of action potentials fired during 600 pairs of positive (NPF preceding PF, red) and 600 pairs of negative conditioning (PF preceding NPF, blue) with an 8 ms interval. ***B***, Cross-correlating the spike trains from positive and negative conditioning shown in ***A*** resulted in a cross-correlation function with a peak at 8 ms and a width at half maximum of 10 ms. ***C***, The majority of cross-correlation functions (n=339) exhibit peak positions coinciding with the interval between the stimuli in the conditioning pair. Results are normalized so that a value of 0 means that the peak position of the cross-correlation function was equal to the interval and negative values indicate that the peak position was closer to 0 ms than expected from the interval used. ***D***, Distribution of widths of cross-correlation functions across the population of units in this study.

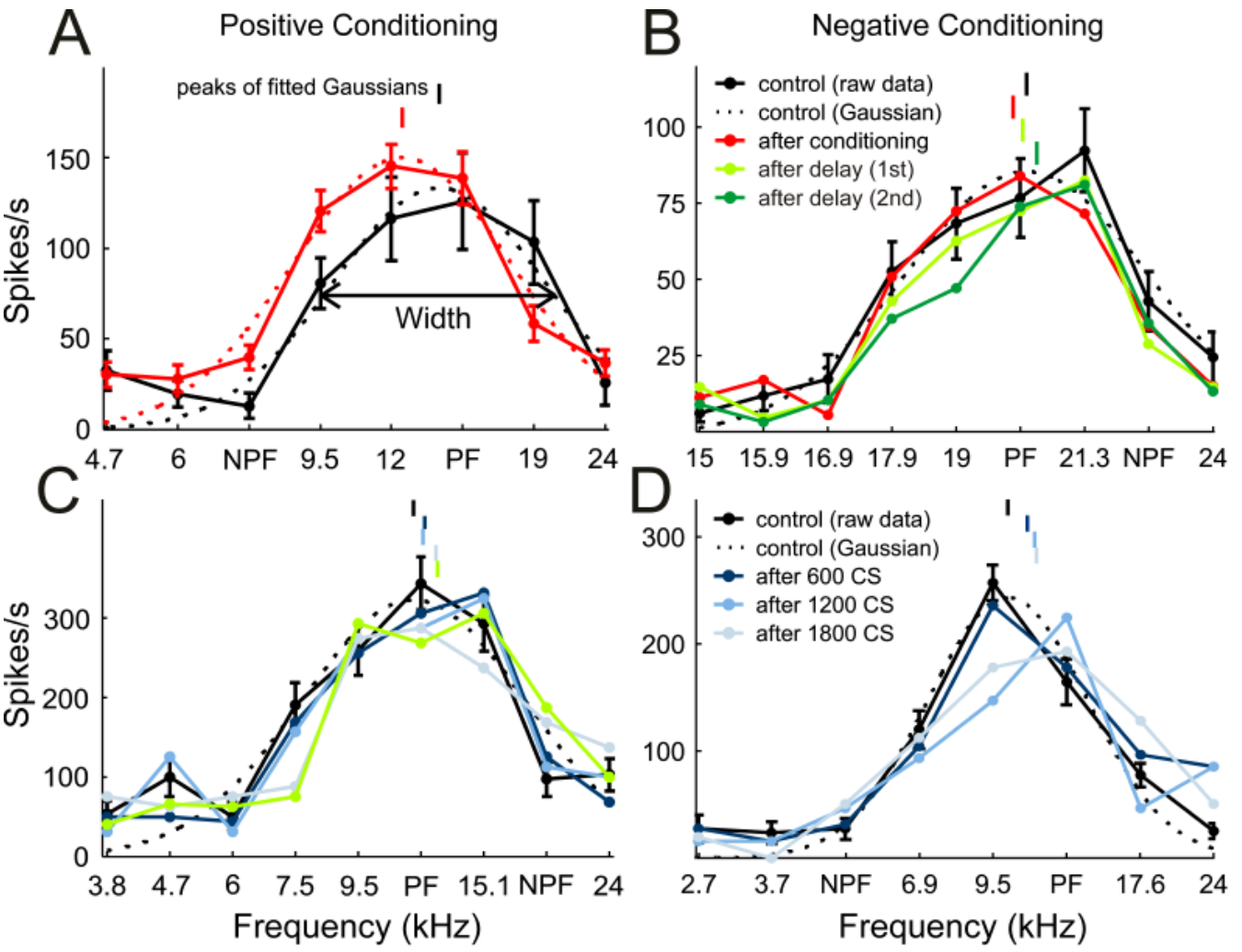

Figure 4.

Example tuning curves. ***A,C***, Positive conditioning examples. ***B,D***, Negative conditioning examples. Pre-conditioning iso-intensity tuning curves are plotted in black. Post-conditioning curves are either shown as the average of all three post-conditioning mapping blocks (plotted in red, as in ***A*** and ***B***), or individually for the first (dark blue), second (mid blue) or third (light blue) post-conditioning mapping blocks, as in ***C*** and ***D***. The persistence of the shifts in the iso-intensity frequency tuning curves is depicted in ***B*** and ***C*** by the post-conditioning curves obtained at different delays (light green, first delay period; dark green, second delay period). Best frequencies (peaks of fitted Gaussians) are indicated by vertical lines above the tuning curves. Gaussian fits (dashed line) and error bars are shown for both pre- and post-conditioning tuning curves in ***A***, but, for clarity, for the pre-conditioning tuning curves only in ***B, C*** and ***D***.

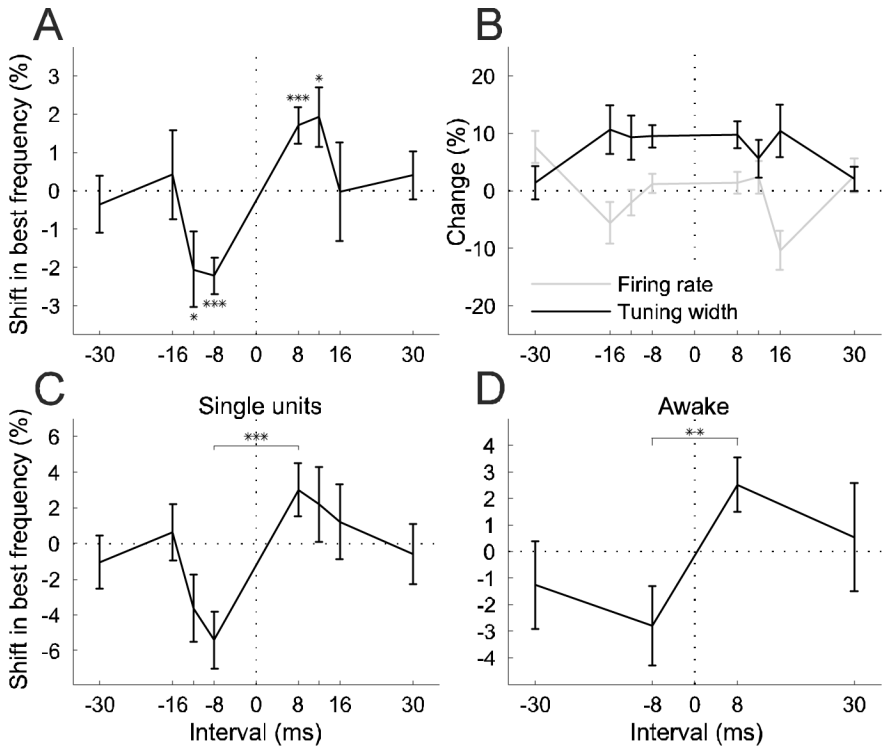

Figure 5.

Temporal specificity of conditioning effects. ***A***, Shifts in best frequency as a function of conditioning interval, normalized by tuning width (sample size ranged from n = 73 to n = 183 for each interval). Negative intervals correspond to negative conditioning and positive intervals to positive conditioning. Negative shifts mean shifts away from the NPF, positive ones shifts towards the NPF. ***B***, Conditioning-dependent changes in tuning width and firing rate for the same population as in ***A***. ***C***, Best frequency shifts for a subpopulation of single units (n = 19-39 for different intervals). ***D***, Best frequency shifts for a population of tuning curves recorded in two alert ferrets (n = 24-30). * = $p < 0.05$, ** = $p < 0.005$, *** = $p < 0.0005$, t-test. Errors bars are ±one standard error of the mean.

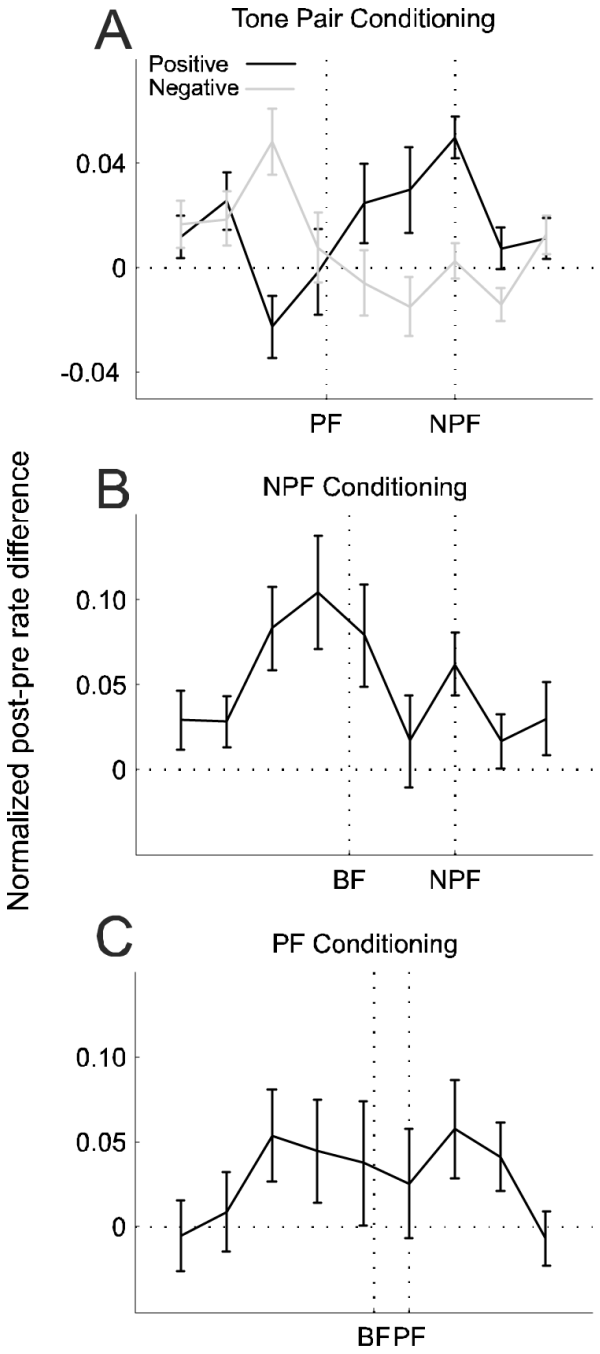

Figure 6.

Average difference-tuning curves. Subtracting pre-conditioning from post-conditioning tuning functions (see Methods) revealed the frequency regions where the response was potentiated or depressed by the conditioning procedures. ***A***, Difference-tuning curves for positive (black, n = 311) and negative (gray, n = 273) conditioning with 8 and 12 ms intervals. While the non-preferred frequency (NPF) is known in each case, because the curves were aligned on this sound frequency, the PF marked on the x-axis represents the average value across all tuning curves. ***B, C***, Difference-tuning curves for single-tone conditioning with an NPF or PF, respectively. The best frequency (BF) position marked on

the x-axis represents the average BF across all curves. Errors bars are ±one standard error of the mean.

Europe PMC Funders Author Manuscripts

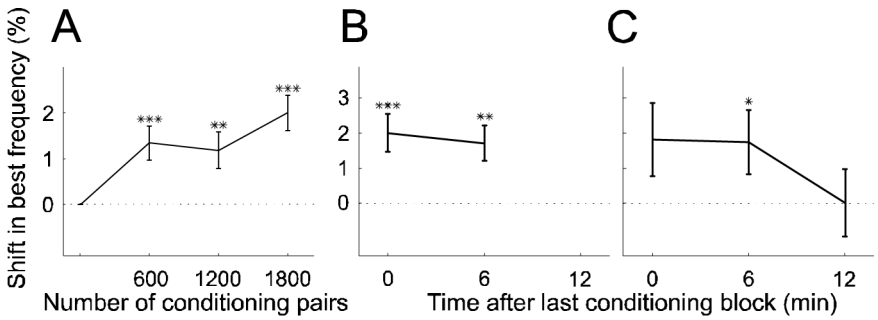

Figure 7.

Time scales of induction and persistence of plasticity. ***A***, Shift in predicted direction as function of the number of conditioning pairs (n = 571). ***B***, In the majority of experiments (n = 350), an additional, fifth, iso-intensity tuning curve was obtained ~6 min after the last conditioning block. ***C***, During some experiments another, sixth, tuning curve was obtained ~12 min after the end of conditioning (n = 100). On average, tuning curve shifts persisted through the fifth mapping block but not the sixth. Only data from conditioning with 8 and 12 ms intervals were considered and the sign of the results from negative conditioning was reversed so that the data could be pooled and plotted as shifts in the predicted direction. * = $p < 0.05$, ** = $p < 0.005$, *** = $p < 0.0005$, t-test. Errors bars are ±one standard error of the mean.

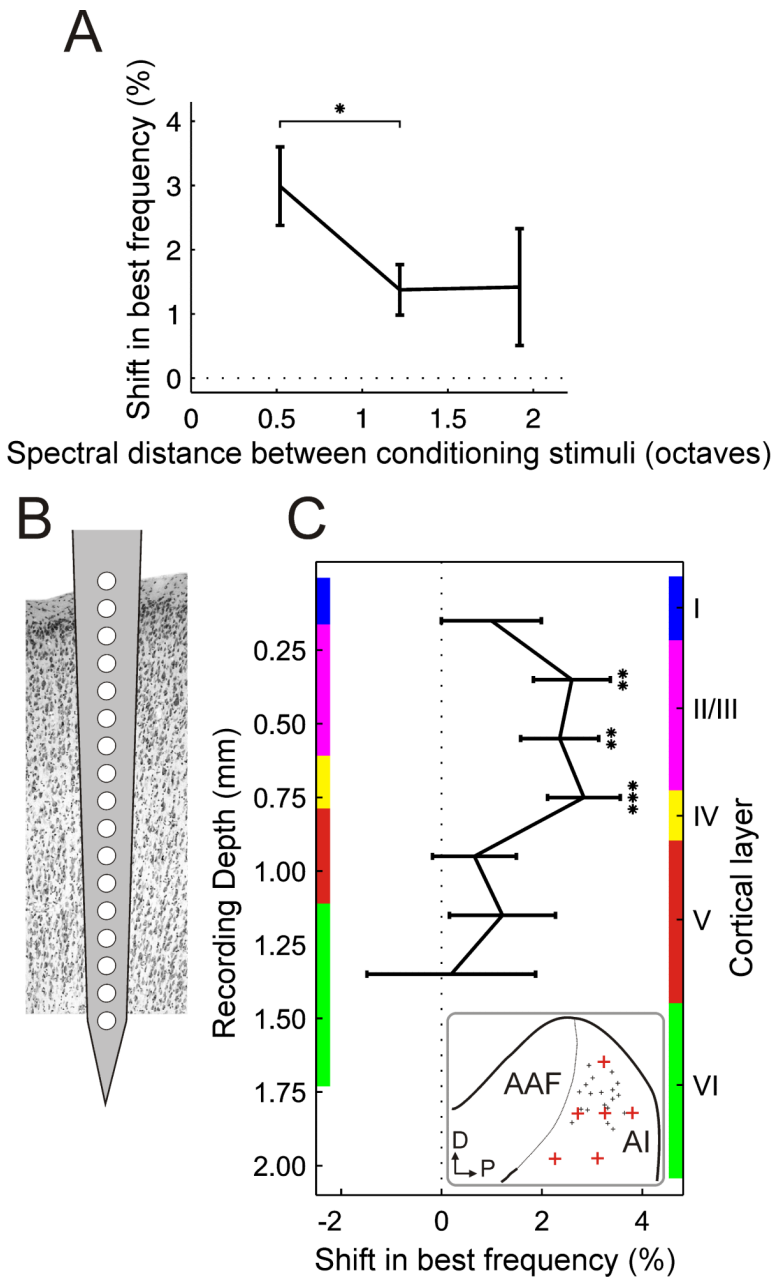

Figure 8.

Two factors affecting stimulus-timing-dependent plasticity. ***A***, Best frequency shifts as a function of the frequency difference between the two stimuli in a conditioning pair (n = 54-326 for different frequency separations). ***B***, Recordings were carried out with 16-site electrodes inserted perpendicular to the cortical surface. ***C***, Best frequency shifts as a function of recording depth. Mean shifts were calculated for pairs of recording sites, excluding sites 1 and 16 from which hardly any recordings were made, and plotted as function of recording depth and cortical layer (n = 26-110 for different depths). Only data from conditioning with 8 and 12 ms intervals were considered and the sign of the results from negative conditioning was reversed so that the data could be pooled and plotted as shifts in the predicted direction. The thickness of the cortical layers was measured at six locations (depicted by the red crosses in the inset; the small black crosses indicate the

locations of the recording sites) over the surface of A1 for two representative ferrets. Colored bars on either side of the graph show the thickness of the cortical layers measured at the thinnest (left) and thickest (right) of those six positions. A1, primary auditory cortex; AAF, anterior auditory field; D, dorsal; P, posterior. * = $p < 0.05$, ** = $p < 0.005$, *** = $p < 0.0005$, t-test. Errors bars are ±one standard error of the mean.

Europe PMC Funders Author Manuscripts

Europe PMC Funders Author Manuscripts

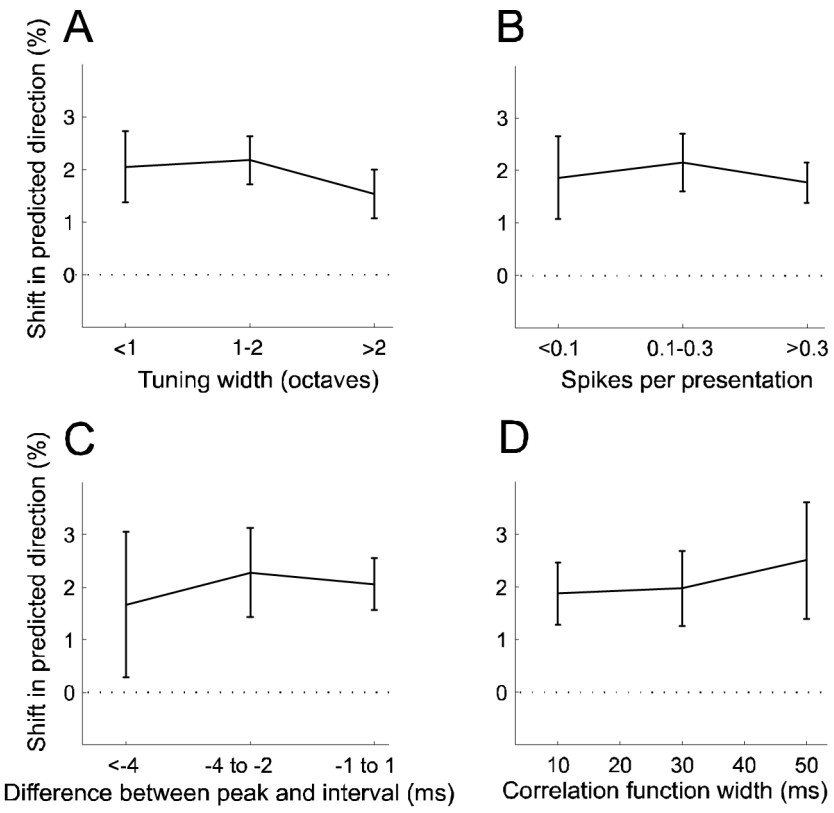

Figure 9.

Dependence of stimulus-timing-depenent plasticity on tuning width, and on the firing rate and temporal precision of responses to conditioning stimuli. ***A***, Shift size as a function of tuning curve width (n = 144-245). ***B***, Shift size as a function of number of spikes fired during presentation of conditioning stimuli (n = 156-267). ***C, D***, Spiking precision was measured using two features of the cross-correlation functions described in Fig. 3: the difference between their peak position and the conditioning interval, and their widths. ***C***, Shift size as a function of the difference between peak position and conditioning interval (n = 51-197). ***D***, Shifts size as a function of cross-correlation width (n = 28-139). Only data from conditioning with 8 and 12 ms intervals were considered and the sign of the results from negative conditioning was reversed so that the data could be pooled and plotted as shifts in the predicted direction. Errors bars are ±one standard error of the mean.

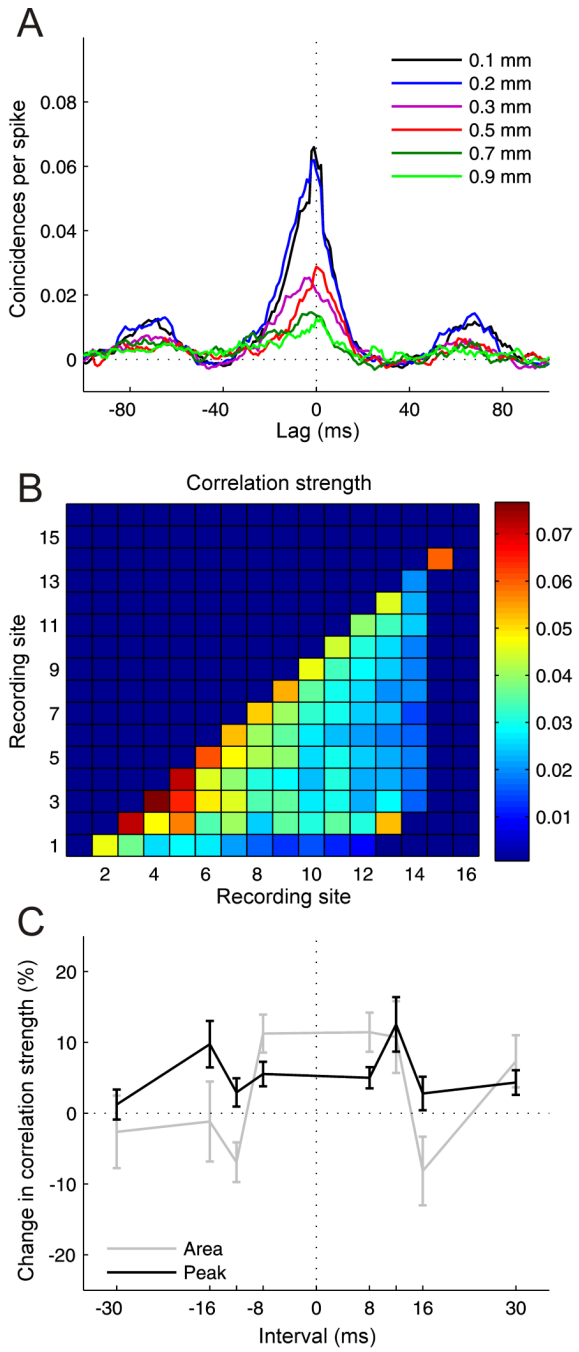

Figure 10.

Results from cross-correlation analysis. ***A***, Cross-correlograms computed between recording sites separated by 0.1 to 0.9 mm on the same multi-site recording probe, smoothed by 3 ms boxcar function. ***B***, Correlation strength measured by the average height of the cross-correlogram peak as a function of recording site combination. ***C***, Changes in correlation strength measured by the area under the cross-correlogram and its peak height as a function of conditioning interval for recording sites separated by up to 0.3 mm (n = 104-292 for different intervals). Errors bars are ±one standard error of the mean.